6 Model Neurons II: Conductances and Morphology

6.1 Levels of Neuron Modeling

In modeling neurons, we must deal with two types of complexity: the intricate interplay of active conductances that makes neuronal dynamics so rich and interesting, and the elaborate morphology that allows neurons to receive and integrate inputs from so many other neurons. The first part of this chapter extends the material presented in chapter 5 by examining single-compartment models with a wider variety of voltage-dependent conductances, and hence a wider range of dynamic behaviors, than the Hodgkin-Huxley model. In the second part of the chapter, we introduce methods used to study the effects of morphology on the electrical characteristics of neurons. An analytic approach known as cable theory is presented first, followed by a discussion of multi-compartment models that permit numerical simulation of complex neuronal structures.

Model neurons range from greatly simplified caricatures to highly detailed descriptions involving thousands of differential equations. Choosing the most appropriate level of modeling for a given research problem requires a careful assessment of the experimental information available and a clear understanding of the research goals. Oversimplified models can, of course, give misleading results, but excessively detailed models can obscure interesting results beneath inessential and unconstrained complexity.

6.2 Conductance-Based Models

The electrical properties of neurons arise from membrane conductances with a wide variety of properties. The basic formalism developed by Hodgkin and Huxley to describe the Na^+ and K^+ conductances responsible for generating action potentials (discussed in chapter 5) is also used to represent most of the additional conductances encountered in neuron modeling. Models that treat these aspects of ionic conductances, known as

conductance-based models, can reproduce the rich and complex dynamics of real neurons quite accurately. In this chapter, we discuss both single- and multi-compartment conductance-based models, beginning with the single-compartment case.

membrane potential equation

To review from chapter 5, the membrane potential of a single-compartment neuron model, V, is determined by integrating the equation

$$c_{\mathrm{m}}\frac{dV}{dt} = -i_{\mathrm{m}} + \frac{I_{\mathrm{e}}}{A}\,, \tag{6.1}$$

with I_{e} the electrode current, A the membrane surface area of the cell, and i_{m} the membrane current. In the following subsections, we present expressions for the membrane current in terms of the reversal potentials, maximal conductance parameters, and gating variables of the different conductances of the models being considered. The gating variables and V comprise the dynamic variables of the model. All the gating variables are determined by equations of the form

gating equations

$$\tau_z(V)\frac{dz}{dt} = z_\infty(V) - z\,, \tag{6.2}$$

where z denotes a generic gating variable. The functions $\tau_z(V)$ and $z_\infty(V)$ are determined from experimental data. For some conductances, these are written in terms of the opening and closing rates $\alpha_z(V)$ and $\beta_z(V)$ (see chapter 5), as

$$\tau_z(V) = \frac{1}{\alpha_z(V)+\beta_z(V)} \quad \text{and} \quad z_\infty(V) = \frac{\alpha_z(V)}{\alpha_z(V)+\beta_z(V)}\,. \tag{6.3}$$

We have written $\tau_z(V)$ and $z_\infty(V)$ as functions of the membrane potential, but for Ca^{2+}-dependent currents they also depend on the internal Ca^{2+} concentration. We call $\alpha_z(V)$, $\beta_z(V)$, $\tau_z(V)$, and $z_\infty(V)$ gating functions. A method for numerically integrating equations 6.1 and 6.2 is described in the appendices of chapter 5.

In the following subsections, some basic features of conductance-based models are presented in a sequence of examples of increasing complexity. We do this to illustrate the effects of various conductances and combinations of conductances on neuronal activity. Different cells (and even the same cell held at different resting potentials) can have quite different response properties due to their particular combinations of conductances. Research on conductance-based models focuses on understanding how neuronal response dynamics arises from the properties of membrane and synaptic conductances, and how the characteristics of different neurons interact when they are coupled in networks.

The Connor-Stevens Model

The Hodgkin-Huxley model of action-potential generation, discussed in chapter 5, was developed on the basis of data from the giant axon of the

squid, and we present a multi-compartment simulation of action-potential propagation using this model in a later section. The Connor-Stevens model (Connor and Stevens, 1971; Connor et al. 1977, which is the model we discuss) provides an alternative description of action-potential generation. Like the Hodgkin-Huxley model, it contains fast Na^+, delayed-rectifier K^+, and leakage conductances. The fast Na^+ and delayed-rectifier K^+ conductances have properties somewhat different from those of the Hodgkin-Huxley model, in particular faster kinetics, so the action potentials are briefer. In addition, the Connor-Stevens model contains an extra K^+ conductance, called the A-current, that is transient. K^+ conductances come in wide variety of different forms, and the Connor-Stevens model involves two of them.

A-type potassium current

The membrane current in the Connor-Stevens model is

$$i_{\rm m} = \overline{g}_L(V - E_{\rm L}) + \overline{g}_{\rm Na} m^3 h (V - E_{\rm Na}) + \overline{g}_K n^4 (V - E_{\rm K}) + \overline{g}_{\rm A} a^3 b (V - E_{\rm A}) , \tag{6.4}$$

where $\overline{g}_{\rm L} = 0.003$ mS/mm^2 and $E_{\rm L}$ = -17 mV are the maximal conductance and reversal potential for the leak conductance; and $\overline{g}_{\rm Na} = 1.2$ mS/mm^2, $\overline{g}_{\rm K} = 0.2$ mS/mm^2, $\overline{g}_{\rm A} = 0.477$ mS/mm^2, $E_{\rm Na}$ = 55 mV, $E_{\rm K}$ = -72 mV, and $E_{\rm A}$ = -75 mV (although the A-current is carried by K^+, the model does not require $E_{\rm A} = E_{\rm K}$). The gating variables, m, h, n, a, and b, are determined by equations of the form 6.2 with the gating functions given in appendix A.

The fast Na^+ and delayed-rectifier K^+ conductances generate action potentials in the Connor-Stevens model just as they do in the Hodgkin-Huxley model (see chapter 5). What is the role of the additional A-current? Figure 6.1 illustrates action-potential generation in the Connor-Stevens model. In the absence of an injected electrode current or synaptic input, the membrane potential of the model remains constant at a resting value of -68 mV. For a constant electrode current greater than a threshold value, the model neuron generates action potentials. Figure 6.1A shows how the firing rate of the model depends on the magnitude of the electrode current relative to the threshold value. The firing rate rises continuously from zero and then increases roughly linearly for currents over the range shown. Figure 6.1B shows an example of action-potential generation for one particular value of the electrode current.

Figure 6.1C shows the firing rate as a function of electrode current for the Connor-Stevens model with the maximal conductance of the A-current set to 0. The leakage conductance and reversal potential have been adjusted to keep the resting potential and membrane resistance the same as in the original model. The firing rate is clearly much higher with the A-current turned off. This is because the deinactivation rate of the A-current limits the rise time of the membrane potential between action potentials. In addition, the transition from no firing for currents less than the threshold value to firing with suprathreshold currents is different when the A-current is eliminated. Without the A-current, the firing rate jumps discontinuously to a nonzero value rather than rising continuously. Neurons with firing

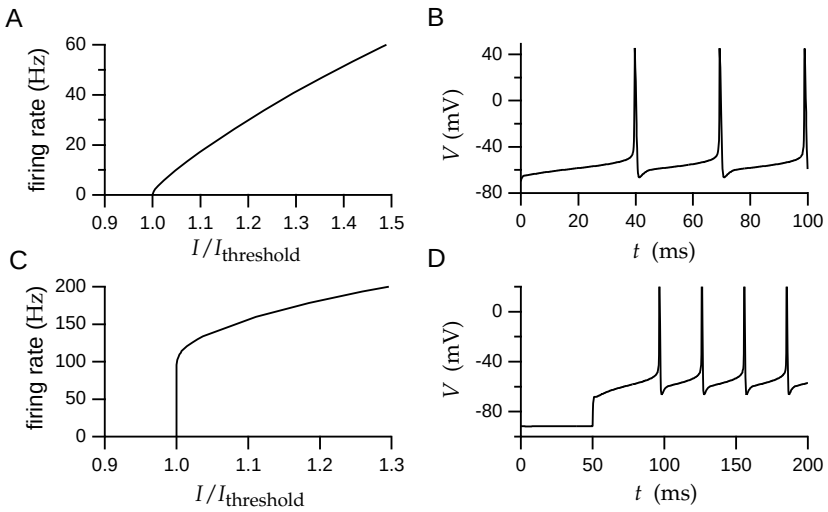

Figure 6.1 Firing of action potentials in the Connor-Stevens model. (A) Firing rate as a function of electrode current. The firing rate rises continuously from 0 as the current increases beyond the threshold value. (B) An example of action potentials generated by constant current injection. (C) Firing rate as a function of electrode current when the A-current is turned off. The firing rate now rises discontinuously from 0 as the current increases beyond the threshold value. (D) Delayed firing due to hyperpolarization. The neuron was held hyperpolarized for a prolonged period by injection of negative current. At $t = 50$ ms, the negative electrode current was switched to a positive value. The A-current delays the occurrence of the first action potential.

type I, type II

rates that rise continuously from 0 as a function of electrode current are called type I, and those with discontinuous jumps in their firing rates at threshold are called type II. An A-current is not the only mechanism that can produce a type I response but, as figures 6.1A and 6.1C show, it plays this role in the Connor-Stevens model. The Hodgkin-Huxley model produces a type II response.

Another effect of the A-current is illustrated in figure 6.1D. Here the model neuron was held hyperpolarized by negative current injection for an extended period of time, and then the current was switched to a positive value. While the neuron was hyperpolarized, the A-current deinactivated, that is, the variable b increased toward 1. When the electrode current switched sign and the neuron depolarized, the A-current first activated and then inactivated. This delayed the first spike following the change in the electrode current.

Postinhibitory Rebound and Bursting

transient Ca^{2+} *conductance*

The range of responses exhibited by the Connor-Stevens model neuron can be extended by including a transient Ca^{2+} conductance. The conductance we use was modeled by Huguenard and McCormick (1992) on the basis of

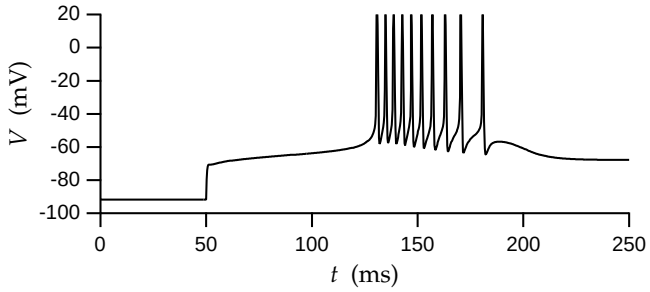

Figure 6.2 A burst of action potentials due to rebound from hyperpolarization. The model neuron was held hyperpolarized for an extended period (until the conductances came to equilibrium) by injection of constant negative electrode current. At $t = 50$ ms, the electrode current was set to 0, and a burst of Na^+ spikes was generated due to an underlying Ca^{2+} spike. The delay in the firing is caused by the presence of the A-current in the model.

data from thalamic relay cells. The membrane current due to the transient Ca^{2+} conductance is expressed as

$$i_{\mathrm{CaT}} = \overline{g}_{\mathrm{CaT}} M^2 H (V - E_{\mathrm{Ca}}) \tag{6.5}$$

with, for the example given here, $\overline{g}_{\mathrm{CaT}} = 0.013$ mS/mm^2 and $E_{\mathrm{Ca}} = 120$ mV. The gating variables for the transient Ca^{2+} conductance are determined from the gating functions in appendix A.

L, T, N and P type Ca^{2+} channels

Several different Ca^{2+} conductances are commonly expressed in neuronal membranes. These are categorized as L, T, N, and P types. L-type Ca^{2+} currents are persistent as far as their voltage dependence is concerned, and they activate at a relatively high threshold. They inactivate due to a Ca^{2+}-dependent rather than voltage-dependent process. T-type Ca^{2+} currents have lower activation thresholds and are transient. N- and P-type Ca^{2+} conductances have intermediate thresholds and are transient and persistent, respectively. They may be responsible for the Ca^{2+} entry that causes the release of transmitter at presynaptic terminals. Entry of Ca^{2+} into a neuron has many secondary consequences ranging from gating Ca^{2+}-dependent channels to inducing long-term modifications of synaptic conductances.

Ca^{2+} spike

burst

A transient Ca^{2+} conductance acts, in many ways, like a slower version of the transient Na^+ conductance that generates action potentials. Instead of producing an action potential, a transient Ca^{2+} conductance generates a slower transient depolarization sometimes called a Ca^{2+} spike. This transient depolarization causes the neuron to fire a burst of action potentials, which are Na^+ spikes riding on the slower Ca^{2+} spike. Figure 6.2 shows such a burst and illustrates one way to produce it. In this example, the model neuron was hyperpolarized for an extended period and then released from hyperpolarization by setting the electrode current to 0. During the prolonged hyperpolarization, the transient Ca^{2+} conductance deinactivated. When the electrode current was set to 0, the resulting depolarization activated the transient Ca^{2+} conductance and generated a burst of

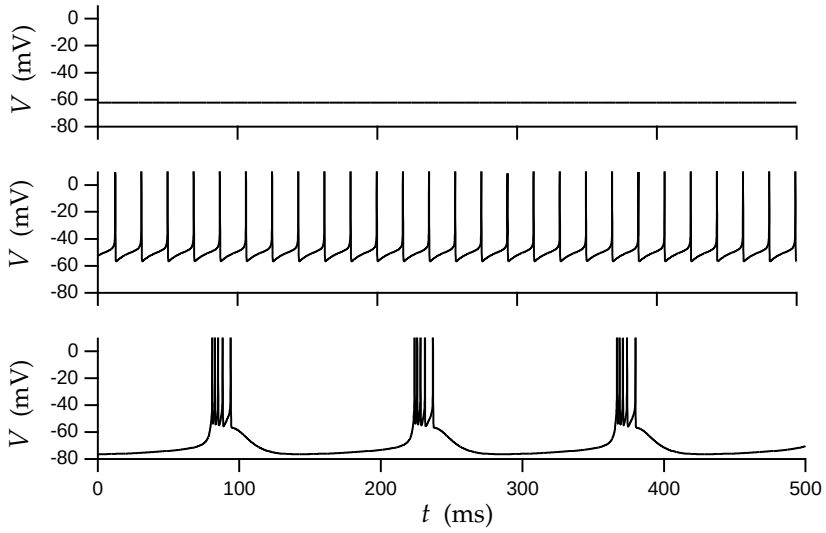

Figure 6.3 Three activity modes of a model thalamic neuron. Upper panel: with no electrode current, the model is silent. Middle panel: when a positive current is injected into the model neuron, it fires action potentials in a regular, periodic pattern. Lower panel: when negative current is injected into the model neuron, it fires action potentials in periodic bursts. (Adapted from Wang, 1994.)

action potentials. The burst in figure 6.2 is delayed due to the presence of the A-current in the Connor-Stevens model to which the Ca^{2+} conductance has been added, and it terminates when the Ca^{2+} conductance inactivates. Generation of action potentials in response to release from hyperpolarization is called postinhibitory rebound because, in a natural setting, the hyperpolarization would be caused by inhibitory synaptic input, not by current injection.

postinhibitory rebound

The transient Ca^{2+} current is an important component of models of thalamic relay neurons. These neurons exhibit different firing patterns in sleep and wakeful states. Action potentials tend to appear in bursts during sleep. Figure 6.3 shows an example of three states of activity of a model thalamic relay cell due to Wang (1994) that has, in addition to fast Na^+, delayed-rectifier K^+, and transient Ca^{2+} conductances, a hyperpolarization-activated mixed-cation conductance and a persistent Na^+ conductance. The cell is silent or fires action potentials in a regular pattern or in bursts, depending on the level of current injection. In particular, injection of small amounts of negative current leads to bursting. This occurs because the hyperpolarization due to the current injection deinactivates the transient Ca^{2+} current and activates the hyperpolarization activated current. The regular firing mode of the middle plot of figure 6.3 is believed to be relevant during wakeful states, when the thalamus is faithfully reporting input from the sensory periphery to the cortex.

thalamic relay neuron

Neurons can fire action potentials either at a steady rate or in bursts even

in the absence of current injection or synaptic input. Periodic bursting is a common feature of neurons in central pattern generators, which are neural circuits that produce periodic patterns of activity to drive rhythmic motor behaviors such as walking, running, or chewing. To illustrate periodic bursting, we consider a model constructed to match the activity of neurons in the crustacean stomatogastric ganglion (STG), a neuronal circuit that controls chewing and digestive rhythms in the foregut of lobsters and crabs. The STG is a model system for investigating the effects of neuromodulators, such as amines and neuropeptides, on the activity patterns of a neural network. Neuromodulators modify neuronal and network behavior by activating, deactivating, or otherwise altering the properties of membrane and synaptic channels. Neuromodulation has a major impact on virtually all neural networks, ranging from peripheral motor pattern generators like the STG to the sensory, motor, and cognitive circuits of the brain.

stomatogastric ganglion

neuromodulator

The model STG neuron contains fast Na^+, delayed-rectifier K^+, A-type K^+, and transient Ca^{2+} conductances similar to those discussed above, although the formulas and parameters used are somewhat different. In addition, the model has a Ca^{2+}-dependent K^+ conductance. Due to the complexity of the model, we do not provide complete descriptions of its conductances except for the Ca^{2+}-dependent K^+ conductance which plays a particularly significant role in the model.

The repolarization of the membrane potential after an action potential is often carried out both by the delayed-rectifier K^+ conductance and by a fast Ca^{2+}-dependent K^+ conductance. Ca^{2+}-dependent K^+ conductances may be voltage dependent, but they are activated primarily by a rise in the level of intracellular Ca^{2+}. A slow Ca^{2+}-dependent K^+ conductance called the after-hyperpolarization (AHP) conductance builds up during sequences of action potentials and typically contributes to the spike-rate adaptation discussed and modeled in chapter 5.

Ca^{2+}-dependent K^+ conductance

after-hyperpolarization conductance

The Ca^{2+}-dependent K^+ current in the model STG neuron is given by

$$i_{\mathrm{KCa}} = \overline{g}_{\mathrm{KCa}} c^4 (V - E_{\mathrm{K}}) , \tag{6.6}$$

where c obeys an equation of the form 6.2, with c_∞ depending on both the membrane potential and the intracellular Ca^{2+} concentration, $[Ca^{2+}]$ (see appendix A). The intracellular Ca^{2+} concentration is computed in this model using a simplified description in which rises in intracellular Ca^{2+} are caused by influx through membrane Ca^{2+} channels, and Ca^{2+} removal is described by an exponential process. The resulting equation for the intracellular Ca^{2+} concentration, $[Ca^{2+}]$, is

$$\frac{d[\mathrm{Ca}^{2+}]}{dt} = -\gamma i_{\mathrm{Ca}} - \frac{[\mathrm{Ca}^{2+}]}{\tau_{\mathrm{Ca}}} . \tag{6.7}$$

Here i_{Ca} is the total Ca^{2+} current per unit area of membrane, τ_{Ca} is the time constant determining the rate at which intracellular Ca^{2+} is removed, and γ is a factor that converts from the electric current due to Ca^{2+} ion flow

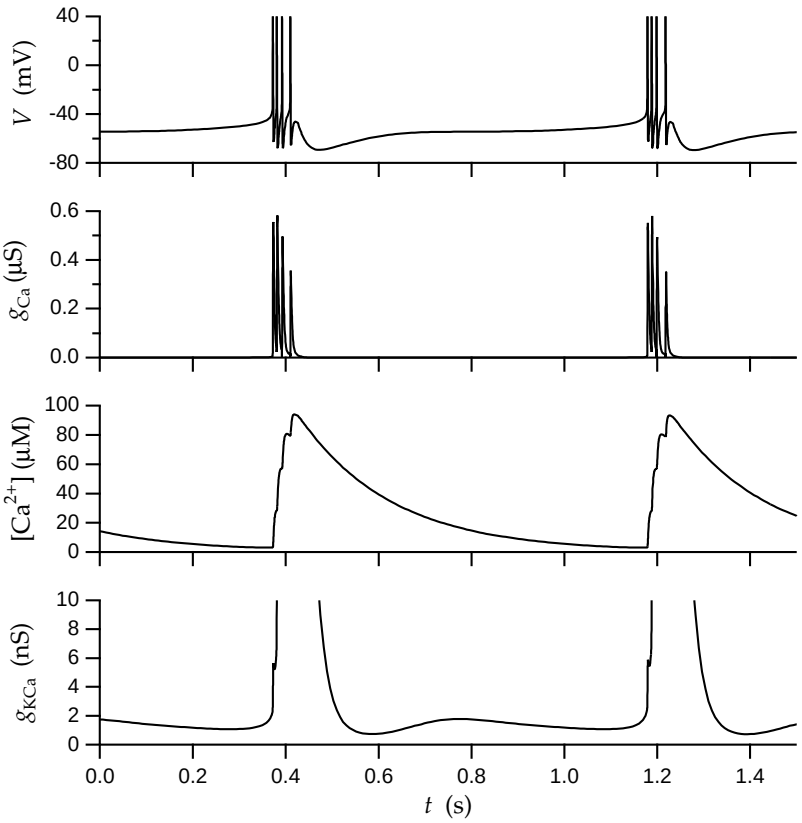

Figure 6.4 Periodic bursting in a model STG neuron. From the top, the panels show the membrane potential, the Ca^{2+} conductance, the intracellular Ca^{2+} concentration, and the Ca^{2+}-dependent K^+ conductance. The Ca^{2+}-dependent K^+ conductance is shown at an expanded scale so the reduction of the conductance due to the falling intracellular Ca^{2+} concentration during the interburst intervals can be seen. In this example, $\tau_{Ca} = 200$ ms. (Simulation by M. Goldman based on a variant of a model of Turrigiano et al., 1995, due to Z. Liu and M. Goldman.)

to the rate at which the Ca^{2+} ion concentration changes within the cell. Because the Ca^{2+} concentration is determined by dividing the number of Ca^{2+} ions in a cell by the total cellular volume and the Ca^{2+} influx is computed by multiplying i_{Ca} by the membrane surface area, γ is proportional to the surface-to-volume ratio for the cell. It also contains a factor that converts from coulombs per second of electrical current to moles per second of Ca^{2+} ions. This factor is $1/(zF)$, where z is the number of charges on the ion ($z = 2$ for Ca^{2+}) and F is the Faraday constant. If, as is normally the case, $[Ca^{2+}]$ is in moles/liter, γ should also contain a factor that converts the volume measure to liters, 10^6 mm^3/liter. Finally, γ is sometimes multiplied by an additional factor that reflects fast intracellular Ca^{2+} buffering. Most of the Ca^{2+} ions that enter a neuron are rapidly bound to intracellular buffers, so only a fraction of the Ca^{2+} current through membrane channels is actually available to change the concentration $[Ca^{2+}]$ of

free Ca^{2+} ions in the cell. This factor is a few percent. The minus sign in front of the γ in equation 6.7 is due to the definition of membrane currents as positive in the outward direction.

Figure 6.4 shows the model STG neuron firing action potentials in bursts. As in the models of figures 6.2 and 6.3, the bursts are transient Ca^{2+} spikes with action potentials riding on top of them. The Ca^{2+} current during these bursts causes a dramatic increase in the intracellular Ca^{2+} concentration. This activates the Ca^{2+}-dependent K^+ current, which, along with the inactivation of the Ca^{2+} current, terminates the burst. The interburst interval is determined primarily by the time it takes for the intracellular Ca^{2+} concentration to return to a low value, which deactivates the Ca^{2+}-dependent K^+ current, allowing another burst to be generated. Although figure 6.4 shows that the conductance of the Ca^{2+}-dependent K^+ current reaches a low value immediately after each burst (due to its voltage dependence), this initial dip is too early for another burst to be generated at that point in the cycle.

6.3 The Cable Equation

Single-compartment models describe the membrane potential over an entire neuron with a single variable. Membrane potentials can vary considerably over the surface of the cell membrane, especially for neurons with long and narrow processes, or if we consider rapidly changing membrane potentials. Figure 6.5A shows the delay and attenuation of an action potential as it propagates from the soma out to the dendrites of a cortical pyramidal neuron. Figure 6.5B shows the delay and attenuation of an excitatory postsynaptic potential (EPSP) initiated in the dendrite by synaptic input as it spreads to the soma. Understanding these features is crucial for determining whether and when a given synaptic input will cause a neuron to fire an action potential.

The attenuation and delay within a neuron are most severe when electrical signals travel down the long, narrow, cablelike structures of dendritic or axonal branches. For this reason, the mathematical analysis of signal propagation within neurons is called cable theory. Dendritic and axonal cables are typically narrow enough that variations of the potential in the radial or axial directions are negligible compared to longitudinal variations. Therefore, the membrane potential along a neuronal cable is expressed as a function of a single longitudinal spatial coordinate x and time, $V(x, t)$, and the basic problem is to solve for this potential.

cable theory

Current flows within a neuron due to voltage gradients. In chapter 5, we discussed how the potential difference across a segment of neuronal cable is related to the longitudinal current flowing down the cable. The longitudinal resistance of a cable segment of length Δx and radius a is given by multiplying the intracellular resistivity r_L by Δx and dividing by the cross-sectional area, πa^2, so that $R_L = r_L \Delta x/(\pi a^2)$. The voltage drop

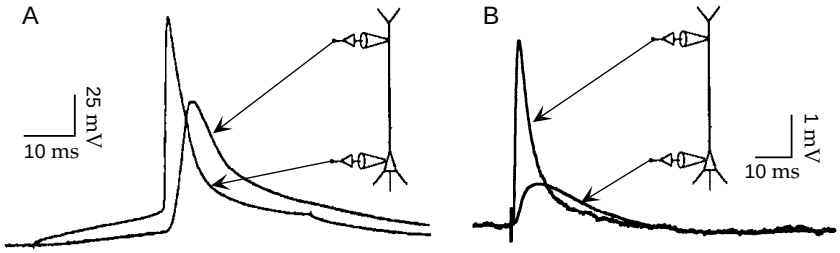

Figure 6.5 Simultaneous intracellular recordings from the soma and apical dendrite of cortical pyramidal neurons in slice preparations. (A) A pulse of current was injected into the soma of the neuron to produce the action potential seen in the somatic recording. The action potential appears delayed and with smaller amplitude in the dendritic recording. (B) A set of axon fibers was stimulated, producing an excitatory synaptic input. The excitatory postsynaptic potential (EPSP) is larger and peaks earlier in the dendrite than in the soma. Note that the scale for the potential is smaller than in A. (A adapted from Stuart and Sakmann, 1994; B adapted from Stuart and Spruston, 1998.)

across this length of cable, $\Delta V = V(x + \Delta x) - V(x)$, is then related to the amount of longitudinal current flow by Ohm's law. In chapter 5, we discussed the magnitude of this current flow, but for the present purposes, we also need to define a sign convention for its direction. We define currents flowing in the direction of increasing x as positive. By this convention, the relationship between ΔV and I_L given by Ohm's law is $\Delta V = -R_L I_L$ or $\Delta V = -r_L \Delta x I_L/(\pi a^2)$. Solving this for the longitudinal current, we find $I_L = -\pi a^2 \Delta V/(r_L \Delta x)$. It is useful to take the limit of this expression for infinitesimally short cable segments, that is, as $\Delta x \to 0$. In this limit, the ratio of ΔV to Δx becomes the derivative $\partial V/\partial x$. We use a partial derivative here because V can also depend on time. Thus, at any point along a cable of radius a and intracellular resistivity r_L, the longitudinal current flowing in the direction of increasing x is

$$I_L = -\frac{\pi a^2}{r_L}\frac{\partial V}{\partial x}. \tag{6.8}$$

The membrane potential $V(x, t)$ is determined by solving a partial differential equation, the cable equation, that describes how the currents entering, leaving, and flowing within a neuron affect the rate of change of the membrane potential. To derive the cable equation, we consider the currents within the small segment shown in figure 6.6. This segment has a radius a and a short length Δx. The rate of change of the membrane potential due to currents flowing into and out of this region is determined by its capacitance. Recall from chapter 5 that the capacitance of a membrane is determined by multiplying the specific membrane capacitance c_m by the area of the membrane. The cylinder of membrane shown in figure 6.6 has a surface area of $2\pi a \Delta x$, and hence a capacitance of $2\pi a \Delta x c_m$. The amount of current needed to change the membrane potential at a rate $\partial V/\partial t$ is thus $2\pi a \Delta x c_m \partial V/\partial t$.

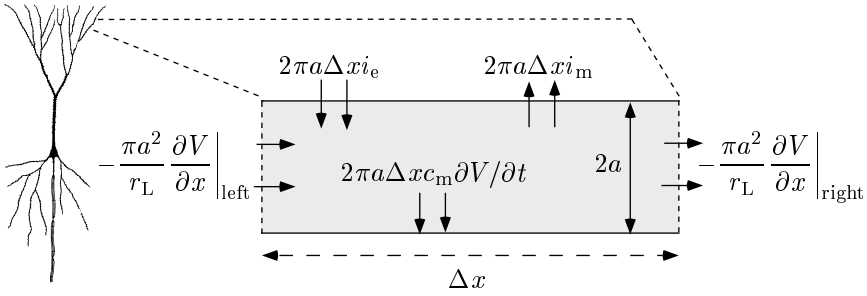

Figure 6.6 The segment of neuron used in the derivation of the cable equation. The longitudinal, membrane, and electrode currents that determine the rate of change of the membrane potential within this segment are denoted. The segment has length Δx and radius a. The expression involving the specific membrane capacitance refers to the rate at which charge builds up on the cell membrane, generating changes in the membrane potential. (The neuron diagram here and in figures 6.15 and 6.16 is from Haberly, 1990.)

All of the currents that can change the membrane potential of the segment being considered are shown in figure 6.6. Current can flow longitudinally into the segment from neighboring segments, and expression 6.8 has been used in figure 6.6 to specify the longitudinal currents at both ends of the segment. Current can flow across the membrane of the segment we are considering through ion and synaptic receptor channels, or through an electrode. The contribution from ion and synaptic channels is expressed as a current per unit area of membrane i_m times the surface area of the segment, $2\pi a\Delta x$. The electrode current is not normally expressed as a current per unit area, but for the present purposes it is convenient to define i_e to be the total electrode current flowing into a given region of the neuronal cable divided by the surface area of that region. The total amount of electrode current being injected into the cable segment of figure 6.6 is then $i_e 2\pi a\Delta x$. Because the electrode current is normally specified by I_e, not by a current per unit area, all the results we obtain will ultimately be re-expressed in terms of I_e. Following the standard convention, membrane and synaptic currents are defined as positive when they are outward, and electrode currents are defined as positive when they are inward.

The cable equation is derived by setting the sum of all the currents shown in figure 6.6 equal to the current needed to charge the membrane. The total longitudinal current entering the cylinder is the difference between the current flowing in on the left and that flowing out on the right. Thus,

$$2\pi a\Delta x c_m \frac{\partial V}{\partial t} = -\left(\frac{\pi a^2}{r_L}\frac{\partial V}{\partial x}\right)\Big|_{left} + \left(\frac{\pi a^2}{r_L}\frac{\partial V}{\partial x}\right)\Big|_{right} - 2\pi a\Delta x(i_m - i_e)\,. \tag{6.9}$$

Dividing both sides of this equation by $2\pi a\Delta x$, we note that the right side involves the term

$$\frac{1}{\Delta x}\left[\left(\frac{\pi a^2}{r_L}\frac{\partial V}{\partial x}\right)\Big|_{right} - \left(\frac{\pi a^2}{r_L}\frac{\partial V}{\partial x}\right)\Big|_{left}\right] \to \frac{\partial}{\partial x}\left(\frac{\pi a^2}{r_L}\frac{\partial V}{\partial x}\right)\,. \tag{6.10}$$

The arrow refers to the limit $\Delta x \to 0$, which we now take. We can move r_L outside the derivative in this equation under the assumption that it is not a function of position. However, the factor of a^2 must remain inside the derivative unless it is independent of x. Substituting the result 6.10 into 6.9, we obtain the cable equation,

cable equation

$$c_m \frac{\partial V}{\partial t} = \frac{1}{2ar_L} \frac{\partial}{\partial x}\left(a^2 \frac{\partial V}{\partial x}\right) - i_m + i_e \,. \tag{6.11}$$

boundary conditions for the cable equation

To determine the membrane potential, equation (6.11) must be augmented by appropriate boundary conditions. The boundary conditions specify what happens to the membrane potential when the neuronal cable branches or terminates. The point at which a cable branches, or equivalently where multiple cable segments join, is called a node. At such a branching node, the potential must be continuous, that is, the functions $V(x,t)$ defined along each of the segments must yield the same result when evaluated at the x value corresponding to the node. In addition, charge must be conserved, which means that the sum of the longitudinal currents entering (or leaving) a node along all of its branches must be 0. According to equation 6.8, the longitudinal current entering a node is proportional to the square of the cable radius times the derivative of the potential evaluated at that point, $a^2 \partial V/\partial x$. The sum of the longitudinal currents entering the node, computed by evaluating these derivatives along each cable segment at the point where they meet at the node, must be 0.

Several different boundary conditions can be imposed at the end of a terminating cable segment. One simple condition is that no current flows out of the end of the cable. By equation 6.8, this means that the spatial derivative of the potential must vanish at a termination point.

Due to the complexities of neuronal membrane currents and morphologies, the cable equation is most often solved numerically, using multicompartmental techniques described later in this chapter. However, it is useful to study analytic solutions of the cable equation in simple cases to get a feel for how different morphological features, such as long dendritic cables, branching nodes, changes in cable radii, and cable ends, affect the membrane potential.

Linear Cable Theory

Before we can solve the cable equation by any method, the membrane current i_m must be specified. We discussed models of various ion channel contributions to the membrane current in chapter 5 and earlier in this chapter. These models typically produce nonlinear expressions that are too complex to allow analytic solution of the cable equation. The analytic solutions we discuss use two rather drastic approximations: synaptic currents are ignored, and the membrane current is written as a linear function of the

membrane potential. Eliminating synaptic currents requires us to examine how a neuron responds to the electrode current i_e. In some cases, electrode current can mimic the effects of a synaptic conductance, although the two are not equivalent. In any case, studying responses to electrode current allows us to investigate the effects of different morphologies on membrane potentials.

Typically, a linear approximation for the membrane current is valid only if the membrane potential stays within a limited range, for example, close to the resting potential of the cell. The resting potential is defined as the potential where no net current flows across the membrane. Near this potential, we approximate the membrane current per unit area as

$$i_m = (V - V_{rest})/r_m \,, \tag{6.12}$$

where V_{rest} is the resting potential and r_m is the specific membrane resistance. It is convenient to define v as the membrane potential relative to the resting potential, $v = V - V_{rest}$, so that $i_m = v/r_m$.

$v = V - V_{rest}$

If the radii of the cable segments used to model a neuron are constant except at branches and abrupt junctions, the factor a^2 in equation 6.11 can be taken out of the derivative and combined with the prefactor $1/2ar_L$ to produce a factor $a/2r_L$ that multiplies the spatial second derivative. With this modification and use of the linear expression for the membrane current, the cable equation for v is

$$c_m \frac{\partial v}{\partial t} = \frac{a}{2r_L}\frac{\partial^2 v}{\partial x^2} - \frac{v}{r_m} + i_e \,. \tag{6.13}$$

It is convenient to multiply this equation by r_m, turning the factor that multiplies the time derivative on the left side into the membrane time constant $\tau_m = r_m c_m$. This also changes the expression multiplying the spatial second derivative on the right side of equation 6.13 to $ar_m/2r_L$. This factor has the dimensions of length squared, and it defines a fundamental length constant for a segment of cable of radius a, the electrotonic length,

electrotonic length λ

$$\lambda = \sqrt{\frac{ar_m}{2r_L}} \,. \tag{6.14}$$

Using the values $r_m = 1$ M$\Omega\cdot$mm^2 and $r_L = 1$ k$\Omega\cdot$mm, a cable of radius $a = 2$ μm has an electrotonic length of 1 mm. A segment of cable with radius a and length λ has a membrane resistance that is equal to its longitudinal resistance, as can be seen from equation 6.14,

R_λ

$$R_\lambda = \frac{r_m}{2\pi a \lambda} = \frac{r_L \lambda}{\pi a^2} \,. \tag{6.15}$$

The resistance R_λ defined by this equation is a useful quantity that enters into a number of calculations.

linear cable equation

Expressed in terms of τ_m and λ, the cable equation becomes

$$\tau_m \frac{\partial v}{\partial t} = \lambda^2 \frac{\partial^2 v}{\partial x^2} - v + r_m i_e \,. \tag{6.16}$$

Equation 6.16 is a linear equation for v similar to the diffusion equation, and it can be solved by standard methods of mathematical analysis. The constants τ_m and λ set the scale for temporal and spatial variations in the membrane potential. For example, the membrane potential requires a time of order τ_m to settle down after a transient, and deviations in the membrane potential due to localized electrode currents decay back to 0 over a length of order λ.

The membrane potential is affected both by the form of the cable equation and by the boundary conditions imposed at branching nodes and terminations. To isolate these two effects, we consider two idealized cases: an infinite cable that does not branch or terminate, and a single branching node that joins three semi-infinite cables. Of course, real neuronal cables are not infinitely long, but the solutions we find are applicable for long cables far from their ends. We determine the potential for both of these morphologies when current is injected at a single point. Because the equation we are studying is linear, the membrane potential for any other spatial distribution of electrode current can be determined by summing solutions corresponding to current injection at different points. The use of point injection to build more general solutions is a standard method of linear analysis. In this context, the solution for a point source of current injection is called a Green's function.

Green's function

An Infinite Cable

In general, solutions to the linear cable equation are functions of both position and time. However, if the current being injected is held constant, the membrane potential settles to a steady-state solution that is independent of time. Solving for this time-independent solution is easier than solving the full time-dependent equation, because the cable equation reduces to an ordinary differential equation in the static case,

$$\lambda^2 \frac{d^2v}{dx^2} = v - r_m i_e \,. \tag{6.17}$$

For the localized current injection we wish to study, i_e is 0 everywhere except within a small region of size Δx around the injection site, which we take to be $x = 0$. Eventually we will let $\Delta x \to 0$. Away from the injection site, the linear cable equation is $\lambda^2 d^2v/dx^2 = v$, which has the general solution $v(x) = B_1 \exp(-x/\lambda) + B_2 \exp(x/\lambda)$ with as yet undetermined coefficients B_1 and B_2. These constant coefficients are determined by imposing boundary conditions appropriate to the particular morphology being considered. For an infinite cable, on physical grounds we simply require that the solution does not grow without bound when $x \to \pm\infty$. This means that we must choose the solution with $B_1 = 0$ for the region $x < 0$ and the solution with $B_2 = 0$ for $x > 0$. Because the solution must be continuous at $x = 0$, we must require $B_1 = B_2 = B$, and these two solutions can be combined into a single expression, $v(x) = B \exp(-|x|/\lambda)$. The remaining task

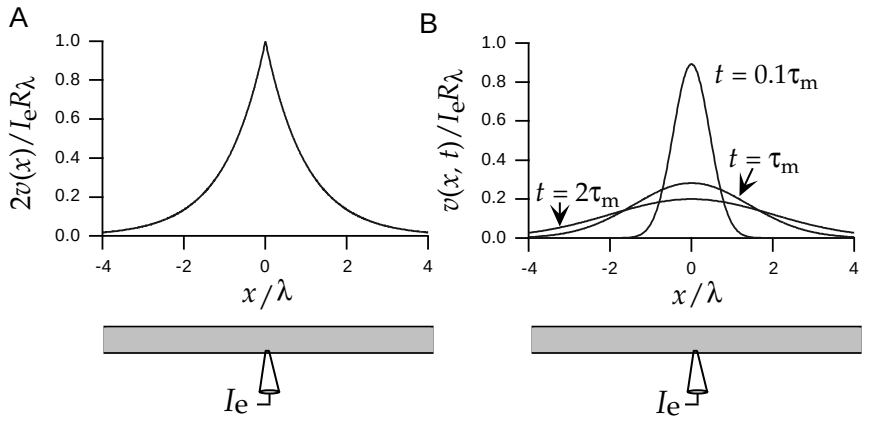

Figure 6.7 The potential for current injection at the point $x = 0$ along an infinite cable. (A) Static solution for a constant electrode current. The potential decays exponentially away from the site of current injection. (B) Time-dependent solution for a δ function pulse of current. The potential is described by a Gaussian function centered at the site of current injection that broadens and shrinks in amplitude over time.

is to determine B, which we do by balancing the current injected with the current that diffuses away from $x = 0$.

In the small region of size Δx around $x = 0$ where the current is injected, the full equation $\lambda^2 d^2v/dx^2 = v - r_m i_e$ must be solved. If the total amount of current injected by the electrode is I_e, the current per unit area injected into this region is $I_e/(2\pi a \Delta x)$. This grows without bound as $\Delta x \to 0$. The first derivative of the membrane potential $v(x) = B\exp(-|x|/\lambda)$ is discontinuous at the point $x = 0$. For small Δx, the derivative at one side of the region we are discussing (at $x = -\Delta x/2$) is approximately B/λ, while at the other side (at $x = +\Delta x/2$) it is $-B/\lambda$. In these expressions, we have used the fact that Δx is small to set $\exp(-|\Delta x|/2\lambda) \approx 1$. For small Δx, the second derivative is approximately the difference between these two first derivatives divided by Δx, which is $-2B/(\lambda \Delta x)$. We can ignore the term v in the cable equation within this small region, because it is not proportional to $1/\Delta x$. Substituting the expressions we have derived for the remaining terms in the equation, we find that $-2\lambda^2 B/(\lambda \Delta x) = -r_m I_e/(2\pi a \Delta x)$, which means that $B = I_e R_\lambda/2$, using R_λ from equation 6.15. Thus, the membrane potential for static current injection at the point $x = 0$ along an infinite cable is

$$v(x) = \frac{I_e R_\lambda}{2} \exp\left(-\frac{|x|}{\lambda}\right). \tag{6.18}$$

According to this result, the membrane potential away from the site of current injection ($x = 0$) decays exponentially with length constant λ (see figure 6.7A). The ratio of the membrane potential at the injection site to the magnitude of the injected current is called the input resistance of the cable. The value of the potential at $x = 0$ is $I_e R_\lambda/2$, indicating that the

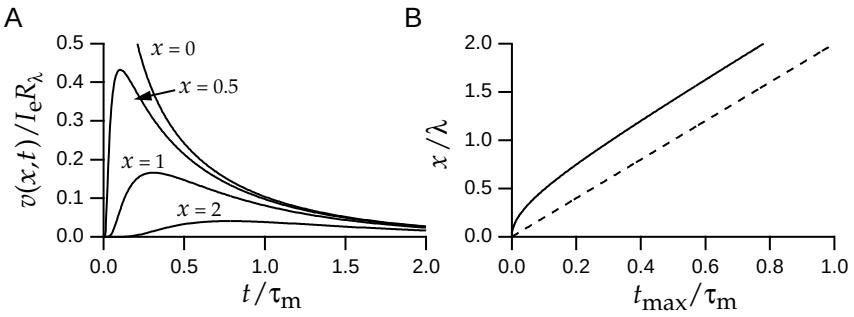

Figure 6.8 Time dependence of the potential on an infinite cable in response to a pulse of current injected at the point $x = 0$ at time $t = 0$. (A) The potential is always largest at the site of current injection. At any fixed point, it reaches its maximum value as a function of time later for measurement sites located farther away from the current source. (B) Movement of the temporal maximum of the potential. The solid line shows the relationship between the measurement location x and the time t_{max} when the potential reaches its maximum value at that location. The dashed line corresponds to a constant velocity $2\lambda/\tau_m$.

infinite cable has an input resistance of $R_\lambda/2$. Each direction of the cable acts like a resistance of R_λ, and these two act in parallel to produce a total resistance half as big. Note that each semi-infinite cable extending from the point $x = 0$ has a resistance equal to a finite cable of length λ.

We now consider the membrane potential produced by an instantaneous pulse of current injected at the point $x = 0$ at the time $t = 0$. Specifically, we consider $i_e = I_e \tau_m \delta(x)\delta(t)/2\pi a$, which means that the current pulse delivers a total charge of $I_e \tau_m$. We do not derive the solution for this case (see Tuckwell, 1988, for example), but simply state the answer,

$$v(x,t) = \frac{I_e R_\lambda}{\sqrt{4\pi t/\tau_m}} \exp\left(-\frac{\tau_m x^2}{4\lambda^2 t}\right) \exp\left(-\frac{t}{\tau_m}\right). \qquad (6.19)$$

In this case, the spatial dependence of the potential is determined by a Gaussian, rather than an exponential function. The Gaussian is always centered around the injection site, so the potential is always largest at $x = 0$. The width of the Gaussian curve around $x = 0$ is proportional to $\lambda\sqrt{t/\tau_m}$. As expected, λ sets the scale for this spatial variation, but the width also grows as the square root of the time measured in units of τ_m. The factor $(4\pi t/\tau_m)^{-1/2}$ in equation 6.19 preserves the total area under this Gaussian curve, but the additional exponential factor $\exp(-t/\tau_m)$ reduces the integrated amplitude over time. As a result, the spatial dependence of the membrane potential is described by a spreading Gaussian function with an integral that decays exponentially (figure 6.7B).

Figure 6.8 shows the solution of equation 6.19 plotted at various fixed positions as a function of time. Figure 6.8A shows that the membrane potential measured farther from the injection site reaches its maximum value at later times. It is important to keep in mind that the membrane potential spreads out from the region $x = 0$; it does not propagate like a wave. Nevertheless,

we can define a type of "velocity" for this solution by computing the time $t_{\max}$ when the maximum of the potential occurs at a given spatial location. This is done by setting the time derivative of $v(x,t)$ in equation 6.19 to 0, giving

$$t_{\max} = \frac{\tau_m}{4}\left(\sqrt{1+4(x/\lambda)^2}-1\right). \tag{6.20}$$

For large x, $t_{\max} \approx x\tau_m/2\lambda$, corresponding to a velocity of $2\lambda/\tau_m$. For smaller x values, the location of the maximum moves faster than this "velocity" would imply (figure 6.8B).

An Isolated Branching Node

To illustrate the effects of branching on the membrane potential in response to a point source of current injection, we consider a single isolated junction of three semi-infinite cables, as shown in the bottom panels of figure 6.9. For simplicity, we discuss the solution for static current injection at a point, but the results generalize directly to the case of time-dependent currents. We label the potentials along the three segments v_1, v_2, and v_3, and label the distance outward from the junction point along any given segment by the coordinate x (although in figure 6.9 a slightly different convention is used). The electrode injection site is located a distance y away from the junction along segment 2. The solution for the three segments is then

$$\begin{aligned} v_1(x) &= p_1 I_e R_{\lambda_1} \exp(-x/\lambda_1 - y/\lambda_2) \\ v_2(x) &= \frac{I_e R_{\lambda_2}}{2}\left[\exp(-|y-x|/\lambda_2) + (2p_2-1)\exp(-(y+x)/\lambda_2)\right] \\ v_3(x) &= p_3 I_e R_{\lambda_3} \exp(-x/\lambda_3 - y/\lambda_2), \end{aligned} \tag{6.21}$$

where, for $i = 1$, 2, and 3,

$$p_i = \frac{a_i^{3/2}}{a_1^{3/2}+a_2^{3/2}+a_3^{3/2}} \quad , \quad \lambda_i = \sqrt{\frac{a_i r_m}{2r_L}} \quad \text{, and} \quad R_{\lambda_i} = \frac{r_L \lambda_i}{\pi a_i^2}. \tag{6.22}$$

Note that the distances x and y appearing in the exponential functions are divided by the electrotonic length of the segment along which the potential is measured or the current is injected. This solution satisfies the cable equation, because it is constructed by combining solutions of the form 6.18. The only term that has a discontinuous first derivative within the range being considered is the first term in the expression for v_2, and this solves the cable equation at the current injection site because it is identical to 6.18. We leave it to the reader to verify that this solution satisfies the boundary conditions $v_1(0) = v_2(0) = v_3(0)$ and $\sum a_i^2 \partial v_i/\partial x = 0$.

Figure 6.9 shows the potential near a junction where a cable of radius 2 μ breaks into two thinner cables of radius 1 μ. In figure 6.9A, current is injected along the thicker cable, and in figure 6.9B it is injected along one of the thinner branches. In both cases, the site of current injection is one

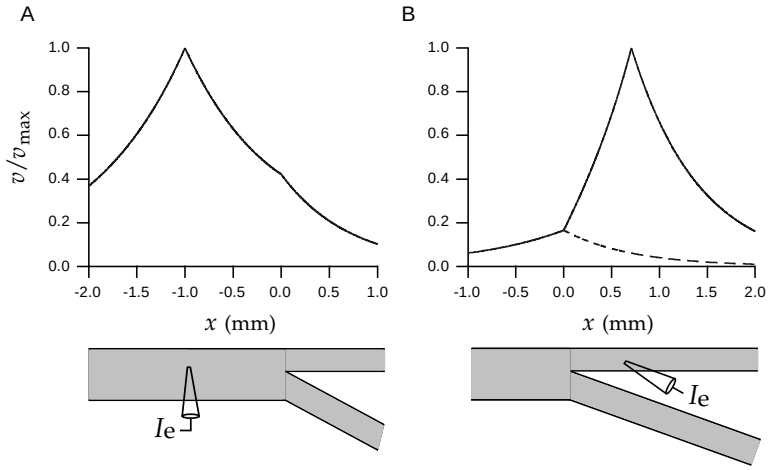

Figure 6.9 The potentials along the three branches of an isolated junction for a current injection site one electrotonic length constant away from the junction. The potential v is plotted relative to v_{max}, which is v at the site of the electrode. The thick branch has a radius of 2 μ and an electrotonic length constant $\lambda = 1$ mm, and the two thin branches have radii of 1 μ and $\lambda = 2^{-1/2}$ mm. (A) Current injection along the thick branch. The potentials along both of the thin branches, shown by the solid curve over the range $x > 0$, are identical. The solid curve over the range $x < 0$ shows the potential on the thick branch where current is being injected. (B) Current injection along one of the thin branches. The dashed line shows the potential along the thin branch where current injection does not occur. The solid line shows the potential along the thick branch for $x < 0$ and along the thin branch receiving the injected current for $x > 0$.

electrotonic length constant away from the junction. The two daughter branches have little effect on the falloff of the potential away from the electrode site in figure 6.9A. This is because the thin branches do not represent a large current sink. The thick branch has a bigger effect on the attenuation of the potential along the thin branch receiving the electrode current in figure 6.9B. This can be seen as an asymmetry in the falloff of the potential on either side of the electrode. Loading by the thick cable segment contributes to a quite severe attenuation between the two thin branches in figure 6.9B. Comparison of figures 6.9A and B reveals a general feature of static attenuation in a passive cable: attenuation near the soma due to potentials arising in the periphery is typically greater than attenuation in the periphery due to potentials arising near the soma.

The Rall Model

The infinite and semi-infinite cables we have considered are clearly mathematical idealizations. We now turn to a model neuron introduced by Rall (1959, 1977) that, though still highly simplified, captures some of the important elements that affect the responses of real neurons. Most neurons receive their synaptic inputs over complex dendritic trees. The integrated

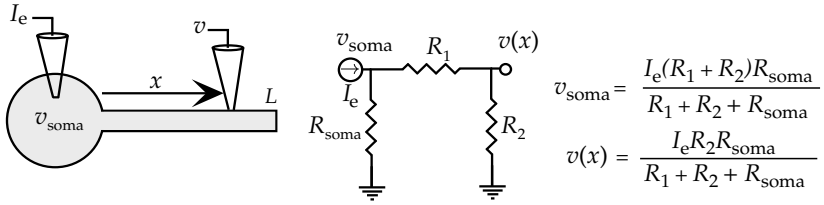

Figure 6.10 The Rall model with static current injected into the soma. The schematic at left shows the recording setup. The potential is measured at the soma and at a distance x along the equivalent cable. The central diagram is the equivalent circuit for this case, and the corresponding formulas for the somatic and dendritic voltages are given at the right. The symbols at the bottom of the resistances R_{soma} and R_2 indicate that $v = 0$ at these points. R_{soma} is the membrane resistance of the soma, and R_1 and R_2 are the resistances given in equations 6.23 and 6.24.

effect of these inputs is usually measured from the soma, and the spike-initiation region of the axon that determines whether the neuron fires an action potential is typically located near the soma. In Rall's model, a compact soma region (represented by one compartment) is connected to a single equivalent cylindrical cable that replaces the entire dendritic region of the neuron (see the schematics in figures 6.10 and 6.12). The critical feature of the model is the choice of the radius and length for the equivalent cable to best match the properties of the dendritic structure being approximated.

The radius a and length L of the equivalent cable are determined by matching two important elements of the full dendritic tree. These are its average length in electrotonic units, which determines the amount of attenuation, and the total surface area, which determines the total membrane resistance and capacitance. The average electrotonic length of a dendrite is determined by considering direct paths from the soma to the terminals of the dendrite. The electrotonic lengths for these paths are constructed by measuring the distance traveled along each of the cable segments traversed in units of the electrotonic length constant for that segment. In general, the total electrotonic length measured by summing these electrotonic segment lengths depends on which terminal of the tree is used as the end point. However, an average value can be used to define an electrotonic length for the full dendritic structure. The length L of the equivalent cable is then chosen so that L/λ is equal to this average electrotonic length, where λ is the length constant for the equivalent cable. The radius of the equivalent cable, which is needed to compute λ, is determined by setting the surface area of the equivalent cable, $2\pi aL$, equal to the surface area of the full dendritic tree.

Under some restrictive circumstances the equivalent cable reproduces the effects of a full tree exactly. Among these conditions is the requirement $a_1^{3/2} = a_2^{3/2} + a_3^{3/2}$ on the radii of any three segments being joined at a node within the tree. Note from equation 6.22 that this condition makes $p_1 = p_2 + p_3 = 1/2$. However, even when the so-called 3/2 law is not exact, the equivalent cable is an extremely useful and often reasonably accurate simplification.

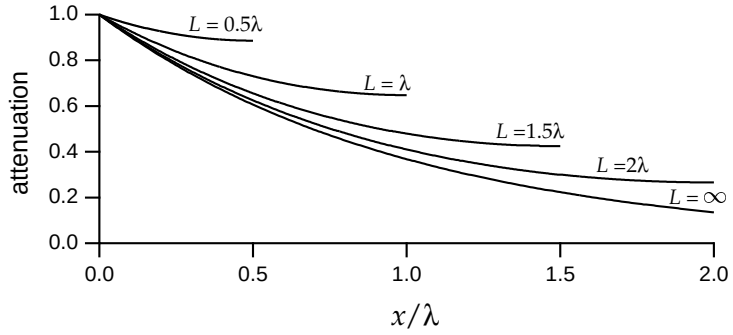

Figure 6.11 Voltage and current attenuation for the Rall model. The attenuation plotted is the ratio of the dendritic voltage to the somatic voltage for the recording setup of figure 6.10, or the ratio of the somatic current to the electrode current for the arrangement in figure 6.12. Attenuation is plotted as a function of x/λ for different equivalent cable lengths.

Figures 6.10 and 6.12 depict static solutions of the Rall model for two different recording configurations, expressed in the form of equivalent circuits. The equivalent circuits are an intuitive way of describing the solution of the cable equation. In figure 6.10, constant current is injected into the soma. The circuit diagram shows an arrangement of resistors that replicates the results of solving the time-independent cable equation (equation 6.17) for the purposes of voltage measurements at the soma, v_{soma}, and at a distance x along the equivalent cable, $v(x)$. The values for these resistances (and similarly the values of R_3 and R_4 given below) are set so that the equivalent circuit reconstructs the solution of the cable equation obtained using standard methods (see, for example, Tuckwell, 1988). R_{soma} is the membrane resistance of the soma, and

$$R_1 = \frac{R_\lambda \left(\cosh\left(L/\lambda\right) - \cosh\left((L-x)/\lambda\right)\right)}{\sinh\left(L/\lambda\right)} \tag{6.23}$$

$$R_2 = \frac{R_\lambda \cosh\left((L-x)/\lambda\right)}{\sinh\left(L/\lambda\right)}. \tag{6.24}$$

Expressions for v_{soma} and $v(x)$, arising directly from the equivalent circuit using standard rules of circuit analysis (see the Mathematical Appendix), are given at the right side of figure 6.10.

The input resistance of the Rall model neuron, as measured from the soma, is determined by the somatic resistance R_{soma} acting in parallel with the effective resistance of the cable, and is $(R_1 + R_2)R_{\text{soma}}/(R_1 + R_2 + R_{\text{soma}})$. The effective resistance of the cable, $R_1 + R_2 = R_\lambda / \tanh(L/\lambda)$, approaches the value R_λ when $L \gg \lambda$. The effect of lengthening a cable saturates when it gets much longer than its electrotonic length. The voltage attenuation caused by the cable is defined as the ratio of the dendritic potential to the somatic potential, and in this case it is given by

$$\frac{v(x)}{v_{\text{soma}}} = \frac{R_2}{R_1 + R_2} = \frac{\cosh\left((L-x)/\lambda\right)}{\cosh\left(L/\lambda\right)}. \tag{6.25}$$

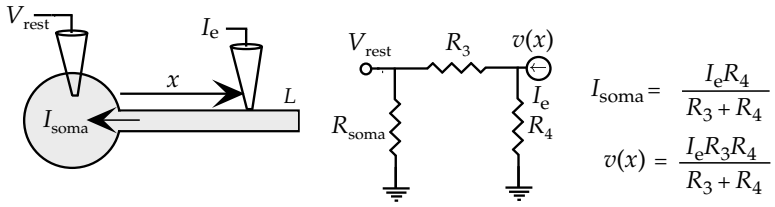

Figure 6.12 The Rall model with static current injected a distance x along the equivalent cable while the soma is clamped at its resting potential. The schematic at left shows the recording setup. The potential at the site of the current injection and the current entering the soma are measured. The central diagram is the equivalent circuit for this case, and the corresponding formulas for the somatic current and dendritic voltage are given at the right. R_{soma} is the membrane resistance of the soma, and R_3 and R_4 are the resistances given in equations 6.26 and 6.27.

This result is plotted in figure 6.11.

Figure 6.12 shows the equivalent circuit for the Rall model when current is injected at a location x along the cable, and the soma is clamped at $v_{soma} = 0$ (or equivalently $V_{soma} = V_{rest}$). The equivalent circuit can be used to determine the current entering the soma and the voltage at the site of current injection. In this case, the somatic resistance is irrelevant because the soma is clamped at its resting potential. The other resistances are

$$R_3 = R_\lambda \sinh(x/\lambda) \tag{6.26}$$

and

$$R_4 = \frac{R_\lambda \sinh(x/\lambda)\cosh((L-x)/\lambda)}{\cosh(L/\lambda) - \cosh((L-x)/\lambda)}. \tag{6.27}$$

The input resistance for this configuration, as measured from the dendrite, is determined by R_3 and R_4 acting in parallel, and is $R_3 R_4/(R_3 + R_4) = R_\lambda \sinh(x/\lambda)\cosh((L-x)/\lambda)/\cosh(L/\lambda)$. When L and x are both much larger than λ, this approaches the limiting value R_λ. The current attenuation is defined as the ratio of the somatic current to the electrode current, and is given by

$$\frac{I_{soma}}{I_e} = \frac{R_4}{R_3 + R_4} = \frac{\cosh((L-x)/\lambda)}{\cosh(L/\lambda)}. \tag{6.28}$$

The inward current attenuation (plotted in figure 6.11) for the recording configuration of figure 6.12 is identical to the outward voltage attenuation for figure 6.10 given by equation 6.25. Equality of the voltage attenuation measured in one direction and the current attenuation measured in the opposite direction is a general feature of linear cable theory.

The Morphoelectrotonic Transform

The membrane potential for a neuron of complex morphology is obviously much more difficult to compute than the simple cases we have

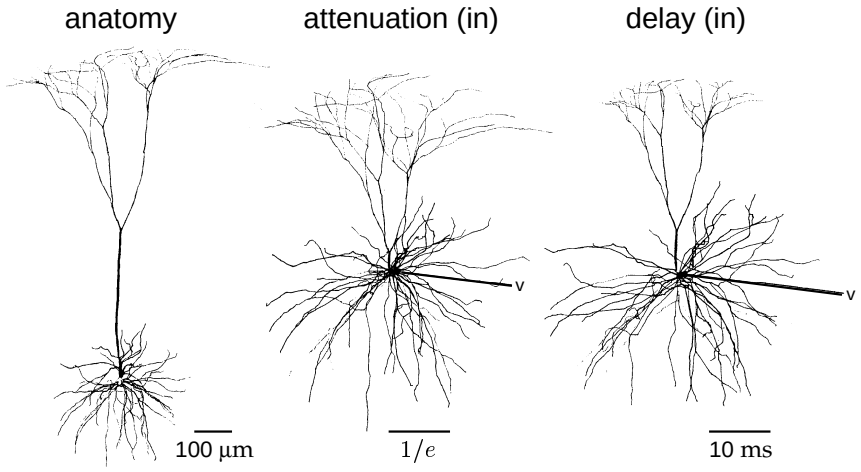

Figure 6.13 The morphoelectrotonic transform of a cortical neuron. The left panel is a normal drawing of the neuron. The central panel is a diagram in which the distance between any point and the soma is proportional to the logarithm of the steady-state attenuation between the soma and that point for static current injected at the terminals of the dendrites. The scale bar denotes the distance corresponding to an attenuation of $\exp(-1)$. In the right panel, the distance from the soma to a given point is proportional to the inward delay, which is the centroid of the soma potential minus the centroid at the periphery when a pulse of current is injected peripherally. The v labels in the diagrams indicate that the reference potential in these cases is the somatic potential. (Adapted from Zador et al, 1995.)

considered. Fortunately, efficient numerical schemes (discussed later in this chapter) exist for generating solutions for complex cable structures. However, even when the solution is known, it is still difficult to visualize the effects of a complex morphology on the potential. Zador et al. (1995; see also Tsai et al., 1994) devised a scheme for depicting the attenuation and delay of the membrane potential for complex morphologies. The voltage attenuation, as plotted in figure 6.11, is not an appropriate quantity to represent geometrically because it is not additive. Consider three points along a cable satisfying $x_1 > x_2 > x_3$. The attenuation between x_1 and x_3 is the product of the attenuation from x_1 to x_2 and from x_2 to x_3, $v(x_1)/v(x_3) = (v(x_1)/v(x_2))(v(x_2)/v(x_3))$. An additive quantity can be obtained by taking the logarithm of the attenuation, due to the identity $\ln(v(x_1)/v(x_3)) = \ln(v(x_1)/v(x_2)) + \ln(v(x_2)/v(x_3))$. The morphoelectrotonic transform is a diagram of a neuron in which the distance between any two points is determined by the logarithm of the ratio of the membrane potentials at these two locations, not by the actual size of the neuron.

morphoelectrotonic transform

Another morphoelectrotonic transform can be used to indicate the amount of delay in the voltage waveform produced by a transient input current. The morphoelectrotonic transform uses a definition of delay different from that used in Figure 6.8B. The delay between any two points is defined as the difference between the centroid, or center of "mass", of the voltage

response at these points. Specifically, the centroid at point x is defined as $\int dt\, t v(x,t) / \int dt\, v(x,t)$. Like the log-attenuation, the delay between any two points on a neuron is represented in the morphoelectrotonic transform as a distance.

Morphoelectrotonic transforms of a pyramidal cell from layer 5 of cat visual cortex are shown in figures 6.13 and 6.14. The left panel of figure 6.13 is a normal drawing of the neuron being studied, the middle panel shows the steady-state attenuation, and the right panel shows the delay. The transformed diagrams correspond to current being injected peripherally, with somatic potentials being compared to dendritic potentials. These figures indicate that, for potentials generated in the periphery, the apical and basal dendrites are much more uniform than the morphology would suggest.

The small neuron diagram at the upper left of figure 6.14 shows attenuation for the reverse situation from figure 6.13, when constant current is injected into the soma and dendritic potentials are compared with the somatic potential. Note how much smaller this diagram is than the one in the central panel of figure 6.13. This illustrates the general feature, mentioned previously, that potentials are attenuated much less in the outward than in the inward direction. This is because the thin dendrites provide less of a current sink for potentials arising from the soma than the soma provides for potentials coming from the dendrites.

The capacitance of neuronal cables causes the voltage attenuation for time-dependent current injection to increase as a function of frequency. Figure 6.14 compares the attenuation of dendritic potentials relative to the somatic potential when constant or sinusoidal current of two different frequencies is injected into the soma. Clearly, attenuation increases dramatically as a function of frequency. Thus, a neuron that appears electrotonically compact for static or low frequency current injection may be not compact when higher frequencies are considered. For example, action potential waveforms, which correspond to frequencies around 500 Hz, are much more severely attenuated within neurons than slower varying potentials.

6.4 Multi-compartment Models

The cable equation can be solved analytically only in relatively simple cases. When the complexities of real membrane conductances are included, the membrane potential must be computed numerically. This is done by splitting the modeled neuron into separate regions or compartments, and approximating the continuous membrane potential $V(x,t)$ by a discrete set of values representing the potentials within the different compartments. This assumes that each compartment is small enough so that there is negligible variation of the membrane potential across it. The precision of such a multi-compartmental description depends on the

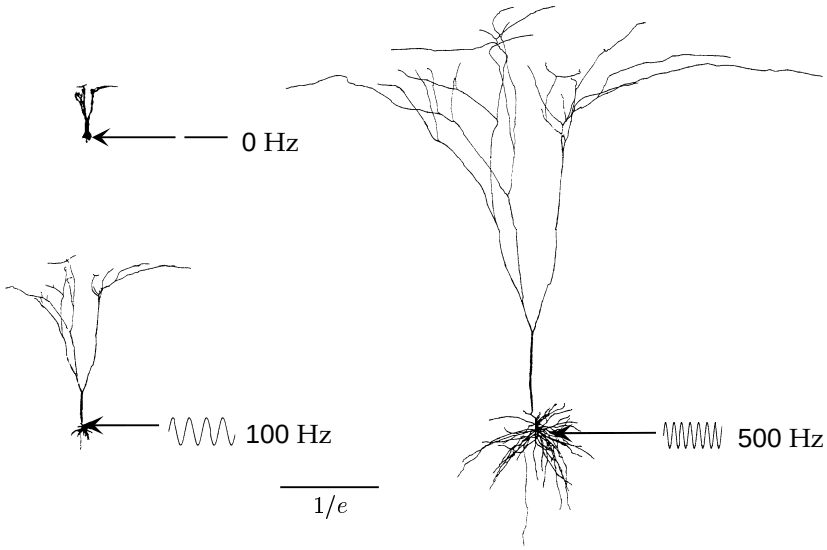

Figure 6.14 Morphoelectrotonic transforms of the same neuron as in figure 6.13 but showing the outward log-attenuation for constant and oscillating input currents. Distances in these diagrams are proportional to the logarithm of the amplitude of the voltage oscillations at a given point divided by the amplitude of the oscillations at the soma when a sinusoidal current is injected into the soma. The upper left panel corresponds to constant current injection, the lower left panel to sinusoidal current injection at a frequency of 100 Hz, and the right panel to an injection frequency of 500 Hz. The scale bar denotes the distance corresponding to an attenuation of $\exp(-1)$. (Adapted from Zador et al., 1995.)

number of compartments used and on their size relative to the length constants that characterize their electrotonic compactness. Figure 6.15 shows a schematic diagram of a cortical pyramidal neuron, along with a series of compartmental approximations of its structure. The number of compartments used can range from thousands, in some models, to one, for the description at the extreme right of figure 6.15.

In a multi-compartment model, each compartment has its own membrane potential V_μ (where μ labels compartments), and its own gating variables that determine the membrane current for compartment μ, $i_{\rm m}^\mu$. Each membrane potential V_μ satisfies an equation similar to 6.1 except that the compartments couple to their neighbors in the multi-compartment structure (figure 6.16). For a nonbranching cable, each compartment is coupled to two neighbors and the equations for the membrane potentials of the compartments are

$$c_{\rm m}\frac{dV_\mu}{dt} = -i_{\rm m}^\mu + \frac{I_{\rm e}^\mu}{A_\mu} + g_{\mu,\mu+1}(V_{\mu+1}-V_\mu) + g_{\mu,\mu-1}(V_{\mu-1}-V_\mu)\,. \quad (6.29)$$

Here $I_{\rm e}^\mu$ is the total electrode current flowing into compartment μ, and A_μ is its surface area. Compartments at the ends of a cable have only one neighbor, and thus only a single term replacing the last two terms in equation 6.29. For a compartment where a cable branches in two, there are

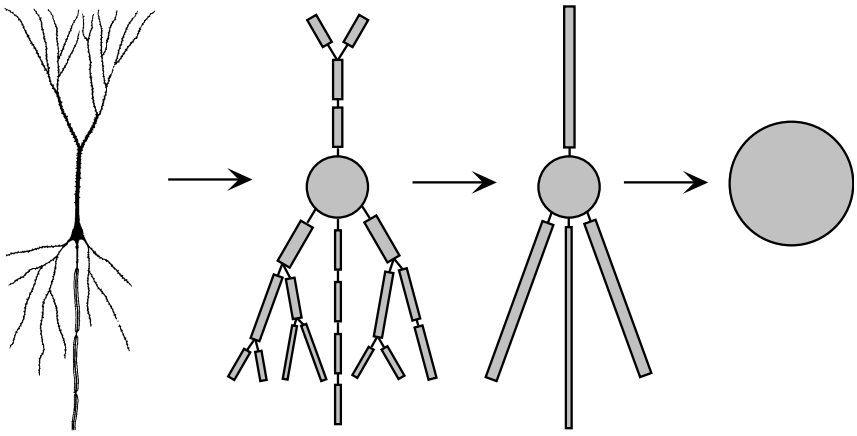

Figure 6.15 A sequence of approximations of the structure of a neuron. The neuron is represented by a variable number of discrete compartments, each representing a region that is described by a single membrane potential. The connectors between compartments represent resistive couplings. The simplest description is the single-compartment model furthest to the right.

three such terms, corresponding to coupling of the branching node to the first compartment in each of the daughter branches.

The constant $g_{\mu,\mu'}$ that determines the resistive coupling from neighboring compartment μ' to compartment μ is determined by computing the current that flows from one compartment to its neighbor due to Ohm's law. For simplicity, we begin by computing the coupling between two compartments that have the same length L and radius a. Using the results of chapter 5, the resistance between two such compartments, measured from their centers, is the intracellular resistivity, r_L times the distance between the compartment centers divided by the cross-sectional area, $r_L L/(\pi a^2)$. The total current flowing from compartment $\mu+1$ to compartment μ is then $\pi a^2 (V_{\mu+1} - V_\mu)/r_L L$. Equation 6.29 for the potential within a compartment μ refers to currents per unit area of membrane. Thus, we must divide the total current from compartment μ' by the surface area of compartment μ, $2\pi aL$, and we find that $g_{\mu,\mu'} = a/(2r_L L^2)$.

The value of $g_{\mu,\mu'}$ is given by a more complex expression if the two neighboring compartments have different lengths or radii. This can occur when a tapering cable is approximated by a sequence of cylindrical compartments, or at a branch point where a single compartment connects with two other compartments, as in figure 6.16. In either case, suppose that compartment μ has length L_μ and radius a_μ, and compartment μ' has length $L_{\mu'}$ and radius $a_{\mu'}$. The resistance between these two compartments is the sum of the two resistances from the middle of each compartment to the junction between them, $r_L L_\mu/(2\pi a_\mu^2) + r_L L_{\mu'}/(2\pi a_{\mu'}^2)$. To compute $g_{\mu,\mu'}$ we invert this expression and divide the result by the total surface area of

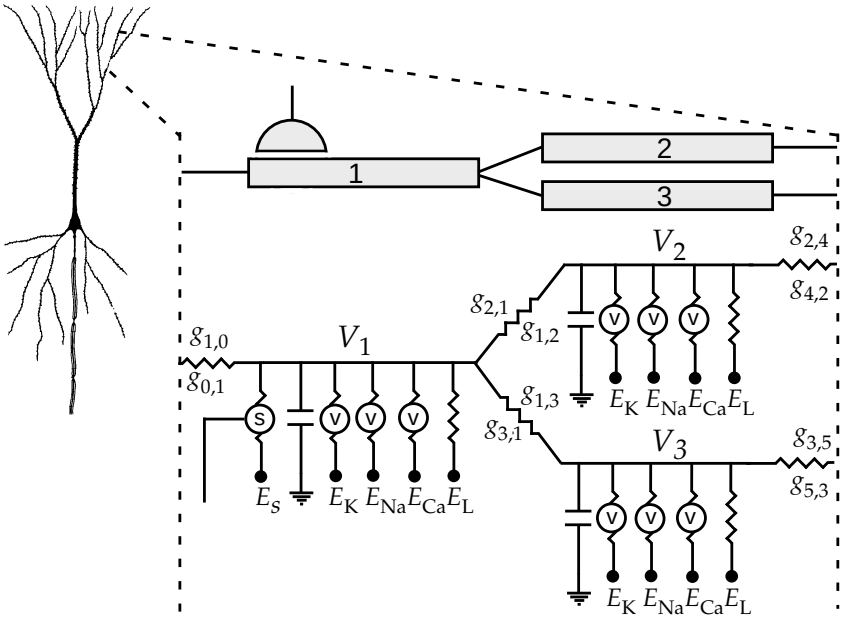

Figure 6.16 A multi-compartment model of a neuron. The expanded region shows three compartments at a branch point where a single cable splits into two. Each compartment has membrane and synaptic conductances, as indicated by the equivalent electrical circuit, and the compartments are coupled together by resistors. Although a single resistor symbol is drawn, note that $g_{\mu,\mu'}$ is not necessarily equal to $g_{\mu',\mu}$.

compartment μ, $2\pi a_\mu L_\mu$, which gives

$$g_{\mu,\mu'} = \frac{a_\mu a_{\mu'}^2}{r_L L_\mu (L_\mu a_{\mu'}^2 + L_{\mu'} a_\mu^2)}. \tag{6.30}$$

Equations 6.29 for all of the compartments of a model determine the membrane potential throughout the neuron with a spatial resolution given by the compartment size. An efficient method for integrating the coupled multi-compartment equations is discussed in appendix B. Using this scheme, models can be integrated numerically with excellent efficiency, even those involving large numbers of compartments. Such integration schemes are built into neuron simulation software packages such as Neuron and Genesis.

Action-Potential Propagation Along an Unmyelinated Axon

As an example of multi-compartment modeling, we simulate the propagation of an action potential along an unmyelinated axon. In this model, each compartment has the same membrane conductances as the single-compartment Hodgkin-Huxley model discussed in chapter 5. The different compartments are joined together in a single nonbranching cable

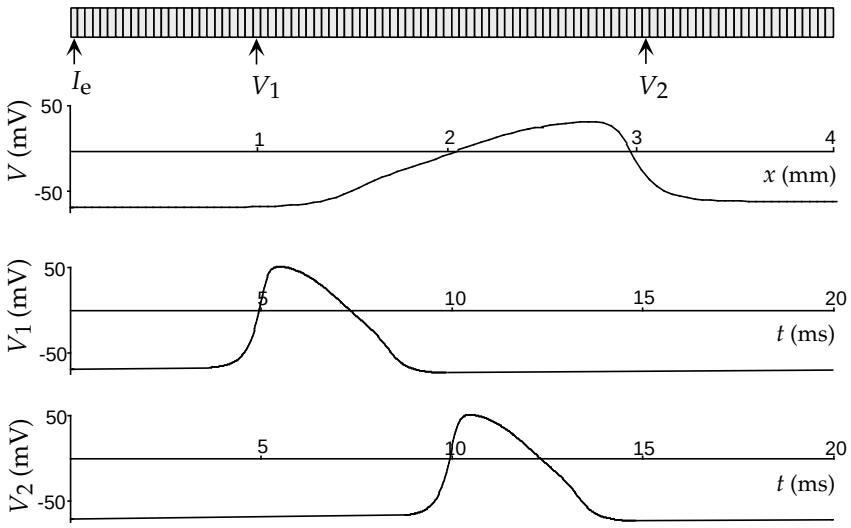

Figure 6.17 Propagation of an action potential along a multi-compartment model axon. The upper panel shows the multi-compartment representation of the axon with 100 compartments. The axon segment shown is 4 mm long and has a radius of 1 μm. An electrode current sufficient to initiate action potentials is injected at the point marked I_e. The panel beneath this shows the membrane potential as a function of position along the axon, at $t = 9.75$ ms. The spatial position in this panel is aligned with the axon depicted above it. The action potential is moving to the right. The bottom two panels show the membrane potential as a function of time at the two locations denoted by the arrows and symbols V_1 and V_2 in the upper panel.

representing a length of axon. Figure 6.17 shows an action-potential propagating along an axon modeled in this way. The action potential extends over more than 1 mm of axon and travels about 2 mm in 5 ms, for a speed of 0.4 m/s.

orthodromic and antidromic propagation

Although action potentials typically move along axons in a direction outward from the soma (called orthodromic propagation), the basic process of action-potential propagation does not favor one direction over the other. Propagation in the reverse direction, called antidromic propagation, is possible under certain stimulation conditions. For example, if an axon is stimulated in the middle of its length, action potentials will propagate in both directions away from the point of stimulation. Once an action potential starts moving along an axon, it does not generate a second action potential moving in the opposite direction because of refractory effects. The region in front of a moving action potential is ready to generate a spike as soon as enough current moves longitudinally down the axon from the region currently spiking to charge the next region up to spiking threshold. However, Na^+ conductances in the region just behind the moving action potential are still partially inactivated, so this region cannot generate another spike until after a recovery period. By the time the trailing region has recovered, the action potential has moved too far away to generate a second spike.

Refractoriness following spiking has a number of other consequences for action-potential propagation. Two action potentials moving in opposite directions that collide annihilate one another because they cannot pass through each other's trailing refractory regions. Refractoriness also keeps action potentials from reflecting off the ends of axon cables, which avoids the impedance matching needed to prevent reflection from the ends of ordinary electrical cables.

The propagation velocity for an action potential along an unmyelinated axon is proportional to the ratio of the electrotonic length constant to the membrane time constant, $\lambda/\tau_m = (a/(2c_m^2 r_L r_m))^{1/2}$. This is proportional to the square root of the axon radius. The square-root dependence of the propagation speed on the axon radius means that thick axons are required to achieve high action-potential propagation speeds, and the squid giant axon is an extreme example. Action-potential propagation can also be sped up by covering the axon with an insulating myelin wrapping, as we discuss next.

Action-Potential Propagation Along a Myelinated Axon

saltatory propagation

Many axons in vertebrates are covered with an insulating sheath of myelin except at gaps, called the nodes of Ranvier, where there is a high density of fast voltage-dependent Na^+ channels (see figure 6.18A). The myelin sheath consists of many layers of glial cell membrane wrapped around the axon. This gives the myelinated region of the axon a very high membrane resistance and a small membrane capacitance. This results in what is called saltatory propagation, in which membrane potential depolarization is transferred passively down the myelin-covered sections of the axon, and action potentials are actively regenerated at the nodes of Ranvier. Figure 6.18A shows an equivalent circuit for a multi-compartment model of a myelinated axon.

We can compute the capacitance of a myelin-covered axon by treating the myelin sheath as an extremely thick cell membrane. Consider the geometry shown in the cross-sectional diagram of figure 6.18B. The myelin sheath extends from the radius a_1 of the axon core to the outer radius a_2. For calculational purposes, we can think of the myelin sheath as being made of a series of thin, concentric cylindrical shells. The capacitances of these shells combine in series to make up the full capacitance of the myelinated axon. If a single layer of cell membrane has thickness d_m and capacitance per unit area c_m, the capacitance of a cylinder of membrane of radius a, thickness Δa, and length L is $c_m 2\pi d_m L a/\Delta a$. According to the rule for capacitors in series, the inverse of the total capacitance is obtained by adding the inverses of the individual capacitances. The capacitance of a myelinated cylinder of length L and the dimensions in figure 6.18B is then obtained by taking the limit $\Delta a \to 0$ and integrating,

$$\frac{1}{C_m} = \frac{1}{c_m 2\pi d_m L}\int_{a_1}^{a_2}\frac{da}{a} = \frac{\ln(a_2/a_1)}{c_m 2\pi d_m L}. \qquad (6.31)$$

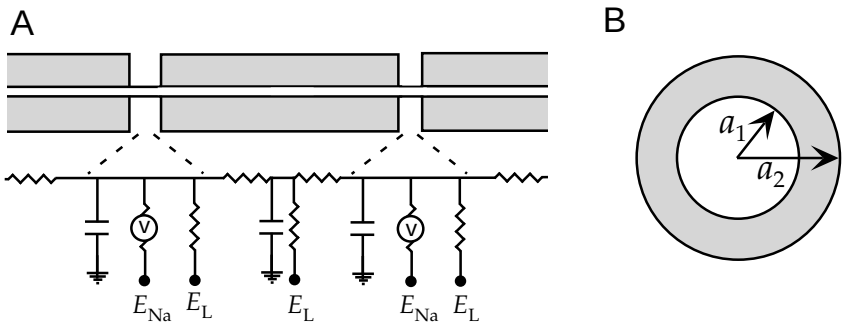

Figure 6.18 A myelinated axon. (A) The equivalent circuit for a multi-compartment representation of a myelinated axon. The myelinated segments are represented by a membrane capacitance, a longitudinal resistance, and a leakage conductance. The nodes of Ranvier also contain a voltage-dependent Na^+ conductance. (B) A cross section of a myelinated axon consisting of a central axon core of radius a_1 and a myelin sheath making the outside radius a_2.

A re-evaluation of the derivation of the linear cable equation earlier in this chapter indicates that the equation describing the membrane potential along the myelinated sections of an axon, in the limit of infinite resistance for the myelinated membrane and with $i_e = 0$, is

$$\frac{C_m}{L}\frac{\partial v}{\partial t} = \frac{\pi a_1^2}{r_L}\frac{\partial^2 v}{\partial x^2}. \tag{6.32}$$

This is equivalent to the diffusion equation, $\partial v/\partial t = D\partial^2 v/\partial x^2$, with diffusion constant $D = \pi a_1^2 L/(C_m r_L) = a_1^2 \ln(a_2/a_1)/(2c_m r_L d_m)$. It is interesting to compute the inner core radius, a_1, that maximizes this diffusion constant for a fixed outer radius a_2. Setting the derivative of D with respect to a_1 to 0 gives the optimal inner radius $a_1 = a_2 \exp(-1/2)$ or $a_1 \approx 0.6a_2$. An inner core fraction of 0.6 is typical for myelinated axons. This indicates that for a given outer radius, the thickness of myelin maximizes the diffusion constant along the myelinated axon segment.

At the optimal ratio of radii, $D = a_2^2/(4ec_m r_L d_m)$, which is proportional to the square of the axon radius. Because of the form of the diffusion equation it obeys with this value of D, v can be written as a function of x/a_2 and t. This scaling implies that the propagation velocity for a myelinated cable is proportional to a_2, that is, to the axon radius, not its square root (as in the case of an unmyelinated axon). Increasing the axon radius by a factor of 4, for example, increases the propagation speed of an unmyelinated cable only by a factor of 2, while it increases the speed for a myelinated cable fourfold.

6.5 Chapter Summary

We continued the discussion of neuron modeling that began in chapter 5 by considering models with more complete sets of conductances and techniques for incorporating neuronal morphology. We introduced A-type K^+, transient Ca^{2+}, and Ca^{2+}-dependent K^+ conductances, and noted their effect on neuronal activity. The cable equation and its linearized version were introduced to examine the effects of morphology on membrane potentials. Finally, multi-compartment models were presented and used to discuss propagation of action potentials along unmyelinated and myelinated axons.

6.6 Appendices

A: Gating Functions for Conductance-Based Models

Connor-Stevens Model

The rate functions used for the gating variables n, m, and h of the Connor-Stevens model, in units of $1/\text{ms}$ with V in units of mV, are

$$\begin{aligned} \alpha_m &= \frac{0.38(V+29.7)}{1-\exp(-0.1(V+29.7))} & \beta_m &= 15.2\exp(-0.0556(V+54.7)) \\ \alpha_h &= 0.266\exp(-0.05(V+48)) & \beta_h &= 3.8/(1+\exp(-0.1(V+18))) \\ \alpha_n &= \frac{0.02(V+45.7)}{1-\exp(-0.1(V+45.7))} & \beta_n &= 0.25\exp(-0.0125(V+55.7))\,. \end{aligned} \tag{6.33}$$

The A-current is described directly in terms of the asymptotic values and τ functions for its gating variables (with τ_a and τ_b in units of ms and V in units of mV),

$$a_\infty = \left(\frac{0.0761\exp(0.0314(V+94.22))}{1+\exp(0.0346(V+1.17))}\right)^{1/3} \tag{6.34}$$

$$\tau_a = 0.3632 + 1.158/(1+\exp(0.0497(V+55.96))) \tag{6.35}$$

$$b_\infty = \left(\frac{1}{1+\exp(0.0688(V+53.3))}\right)^4 \tag{6.36}$$

and

$$\tau_b = 1.24 + 2.678/(1+\exp(0.0624(V+50)))\,. \tag{6.37}$$

Transient Ca^{2+} Conductance

The gating functions used for the variables M and H in the transient Ca^{2+} conductance model we discussed, with V in units of mV and τ_M and τ_H in ms, are

$$M_\infty = \frac{1}{1 + \exp\left(-(V + 57)/6.2\right)} \tag{6.38}$$

$$H_\infty = \frac{1}{1 + \exp\left((V + 81)/4\right)} \tag{6.39}$$

$$\tau_M = 0.612 + \left(\exp\left(-(V + 132)/16.7\right) + \exp\left((V + 16.8)/18.2\right)\right)^{-1} \tag{6.40}$$

and

$$\tau_H = \begin{cases} \exp\left((V + 467)/66.6\right) & \text{if } V < -80 \text{ mV} \\ 28 + \exp\left(-(V + 22)/10.5\right) & \text{if } V \geq -80 \text{ mV}\,. \end{cases} \tag{6.41}$$

Ca^{2+}-dependent K^+ Conductance

The gating functions used for the Ca^{2+}-dependent K^+ conductance we discussed, with V in units of mV and τ_c in ms, are

$$c_\infty = \left(\frac{[Ca^{2+}]}{[Ca^{2+}] + 3\mu\text{M}}\right) \frac{1}{1 + \exp(-(V + 28.3)/12.6)} \tag{6.42}$$

and

$$\tau_c = 90.3 - \frac{75.1}{1 + \exp(-(V + 46)/22.7)}\,. \tag{6.43}$$

B: Integrating Multi-compartment Models

Multi-compartment models are defined by a coupled set of differential equations (equation 6.29), one for each compartment. There are also gating variables for each compartment, but these involve only the membrane potential (and possibly Ca^{2+} concentration) within that compartment, and integrating their equations can be handled as in the single-compartment case using the approach discussed in appendix B of chapter 5. Integrating the membrane potentials for the different compartments is more complex because they are coupled to each other.

Equation 6.29, for the membrane potential within compartment μ, can be written in the form

$$\frac{dV_\mu}{dt} = B_\mu V_{\mu-1} + C_\mu V_\mu + D_\mu V_{\mu+1} + F_\mu\,, \tag{6.44}$$

where

$$B_\mu = c_m^{-1} g_{\mu,\mu-1}\,, \quad C_\mu = -c_m^{-1}\Big(\sum_i g_i^\mu + g_{\mu,\mu+1} + g_{\mu,\mu-1}\Big)\,,$$
$$D_\mu = c_m^{-1} g_{\mu,\mu+1}\,, \quad F_\mu = c_m^{-1}\Big(\sum_i g_i^\mu E_i + I_e^\mu / A_\mu\Big)\,. \tag{6.45}$$

Note that the gating variables and other parameters have been absorbed into the values of the coefficients B_μ, C_μ, D_μ, and F_μ in this equation. Equation 6.44, with μ running over all of the compartments of the model, generates a set of coupled differential equations. Because of the coupling between compartments, we cannot use the method discussed in appendix A of chapter 5 to integrate these equations. Instead, we present another method that shares some of the positive features of that approach. The Runge-Kutta method, which is a standard numerical integrator, is poorly suited for this application and is likely to run orders of magnitude slower than the method described below.

Two of the most important features of an integration method are accuracy and stability. Accuracy refers to how closely numerical finite-difference methods reproduce the exact solution of a differential equation as a function of the integration step size Δt. Stability refers to what happens when Δt is chosen to be excessively large and the method starts to become inaccurate. A stable integration method will degrade smoothly as Δt is increased, producing results of steadily decreasing accuracy. An unstable method, on the other hand, will at some point display a sudden transition and generate wildly inaccurate results. Given the tendency of impatient modelers to push the limits on Δt, it is highly desirable to have a method that is stable.

Defining

$$V_\mu(t + \Delta t) = V_\mu(t) + \Delta V_\mu\,, \tag{6.46}$$

the finite difference form of equation 6.44 gives the update rule

$$\Delta V_\mu = \big(B_\mu V_{\mu-1}(t) + C_\mu V_\mu(t) + D_\mu V_{\mu+1}(t) + F_\mu\big)\,\Delta t\,, \tag{6.47}$$

which is how ΔV_μ is computed using the so-called Euler method. This method is both inaccurate and unstable. The stability of the method can be improved dramatically by evaluating the membrane potentials on the right side of equation 6.47 not at time t, but at a later time $t + z\Delta t$, so that

$$\Delta V_\mu = \big(B_\mu V_{\mu-1}(t+z\Delta t) + C_\mu V_\mu(t+z\Delta t) + D_\mu V_{\mu+1}(t+z\Delta t) + F_\mu\big)\,\Delta t\,. \tag{6.48}$$

Two such methods are predominantly used, the reverse Euler method, for which $z = 1$, and the Crank-Nicholson method with $z = 0.5$. The reverse Euler method is the more stable of the two and the Crank-Nicholson is the more accurate. In either case, ΔV_μ is determined from equation 6.48. These methods are called implicit because equation 6.48 must be solved

to determine ΔV_μ. To do this, we write $V_\mu(t + z\Delta t) \approx V_\mu(t) + z\Delta V_\mu$ and likewise for $V_{\mu\pm1}$. Substituting this into equation 6.48 gives

$$\Delta V_\mu = b_\mu \Delta V_{\mu-1} + c_\mu \Delta V_\mu + d_\mu \Delta V_{\mu+1} + f_\mu \,, \tag{6.49}$$

where

$$\begin{aligned} b_\mu &= B_\mu z\Delta t \,, \quad c_\mu = C_\mu z\Delta t \,, \quad d_\mu = D_\mu z\Delta t \,, \\ f_\mu &= (F_\mu + B_\mu V_{\mu-1}(t) + C_\mu V_\mu(t) + D_\mu V_{\mu+1}(t))\Delta t \,. \end{aligned} \tag{6.50}$$

Equation 6.49 for all μ values provides a set of coupled linear equations for the quantities ΔV_μ. An efficient method exists for solving these equations (Hines, 1984; Tuckwell, 1988). We illustrate the method for a single, nonbranching cable that begins at compartment $\mu = 1$, so that $b_1 = 0$, and ends at compartment $\mu = N$, so $d_N = 0$. The method consists of solving equation 6.49 for ΔV_μ in terms of $\Delta V_{\mu+1}$ sequentially, starting at one end of the cable and proceeding to the other end. For example, if we start the procedure at compartment 1, ΔV_1 can be expressed as

$$\Delta V_1 = \frac{d_1 \Delta V_2 + f_1}{1 - c_1}. \tag{6.51}$$

Substituting this into the equation 6.49 for $\mu = 2$ gives

$$\Delta V_2 = c_2' \Delta V_2 + d_2 \Delta V_3 + f_2' \,, \tag{6.52}$$

where $c_2' = c_2 + b_2 d_1/(1 - c_1)$ and $f_2' = f_2 + b_2 f_1/(1 - c_1)$. We now repeat the procedure going down the cable. At each stage, we solve for $\Delta V_{\mu-1}$ in terms of ΔV_μ, finding

$$\Delta V_{\mu-1} = \frac{d_{\mu-1} \Delta V_\mu + f_{\mu-1}'}{1 - c_{\mu-1}'} \,, \tag{6.53}$$

where

$$c_{\mu+1}' = c_{\mu+1} + \frac{b_{\mu+1} d_\mu}{1 - c_\mu'} \tag{6.54}$$

and

$$f_{\mu+1}' = f_{\mu+1} + \frac{b_{\mu+1} f_\mu'}{1 - c_\mu'} \,. \tag{6.55}$$

Finally, when we get to the end of the cable, we can solve for

$$\Delta V_N = \frac{f_N'}{1 - c_N'} \tag{6.56}$$

because $d_N = 0$.

The procedure for computing all the ΔV_μ is the following. Define $c_1' = c_1$ and $f_1' = f_1$ and iterate equations 6.54 and 6.55 down the length of the

cable to define all the c' and f' parameters. Then solve for ΔV_N from equation 6.56 and iterate back up the cable, solving for the ΔV's using 6.53. This process takes only $2N$ steps.

We leave the extension of this method to the case of a branched cable as an exercise for the reader. The general procedure is similar to the one we presented for a nonbranching cable. The equations are solved by starting at the ends of the branches and moving in toward their branching node, then continuing on as for a nonbranching cable, and finally reversing direction and completing the solution moving in the opposite direction along the cable and its branches.

6.7 Annotated Bibliography

Many of the references for chapter 5 apply to this chapter as well, including **Jack et al. (1975)**, **Tuckwell (1988)**, **Johnston & Wu (1995)**, **Koch & Segev (1998)**, **Koch (1998)**, **Hille (1992)**, and **Mascagni & Sherman (1998)**. **Rall (1977)** describes cable theory, the equivalent cable model of dendritic trees, and the 3/2 law. The solution of equation 6.21 can be constructed using the set of rules for solving the linear cable equation on arbitrary trees found in Abbott (1992; see also Abbott et al., 1991). **Marder & Calabrese (1996)** reviews neuromodulation.

Two freely available software packages for detailed neuronal modeling are in wide use, `Neuron` (see Hines & Carnevale, 1997) and `Genesis` (see Bower & Beeman, 1998). These are available at `http://www.neuron.yale.edu` and `http://genesis.bbb.caltech.edu/GENESIS/genesis.html`.